Article

Journal of Industrial Textiles

2015, Vol. 44(4) 639–661

DOI: 10.1177/1528083713516665
jit.sagepub.com
SAGE

Investigation of pumice stone powder coating of multilayer surfaces in relation to acoustic and thermal insulation

Seyda Canbolat[1], Dilek Kut[2] and Habip Dayioglu[1]

Abstract

In this study, production of multilayer surfaces for acoustic and thermal insulation was investigated. After the optimum textile materials had been chosen to provide acoustic and thermal insulation, surfaces were created using different relative methods in this field. Sublayer nonwoven produced from slotted polyester fiber was combined with two different top layers of fabrics, one of which was the top layer of fabric woven from plain weave obtained from texture yarns, which, in turn, was produced from hollow polypropylene, and the other was plain weave obtained from texture weft yarn, which was produced from conventional polypropylene fibers separately. Subsequently, these two different surfaces were combined with polyurethane-based material. Pumice stone powder in three different concentrations and two different sizes was added to enhance acoustic and thermal insulation, after which the sublayer had been coated with an adhesive material to produce multilayer adhesive force and adherence to the wall. Consequently, air permeability, sound absorption, and thermal conductivity coefficients of multilayer surfaces were researched with regard to the type of top layer of fabrics, concentration, and particle size of pumice stone powder. The results demonstrate that the properties of multilayer surfaces concerning acoustic and thermal insulation increase with the increasing concentration of pumice stone powder and with the decreasing sizes of pumice stone particles. In addition, air permeability of multilayer surfaces was ensued to decrease with the increasing concentration as well as particle size of pumice stone powder.

[1]Faculty of Engineering and Design, Department of Textile Engineering, Istanbul Commerce University, Istanbul, Turkey
[2]Faculty of Engineering and Architecture, Textile Engineering, Uludag University, Bursa, Turkey

Corresponding author:
Seyda Canbolat, Faculty of Engineering and Design, Department of Textile Engineering, Istanbul Commerce University, Kucukyali E5 Crossroad, Kucukyali, Istanbul 34840, Turkey.
Email: scanbolat@ticaret.edu.tr

Keywords
Acoustic insulation, adhesion, air permeability, thermal insulation, pumice stone

Introduction

More particularly in smaller areas, modern city life has been enhancing human comfort, one major requirement of which is tranquility and prevention of noise pollution. In this regard, technologies of acoustic insulation in the newly built buildings are frequently employed. Another requirement of human comfort in the living space is to overcome problems regarding thermal insulation systems in buildings, which otherwise would have increased the heating costs. For these reasons, research has been conducted for the development of acoustic and thermal insulation in the living space. Rubber, tea leaf fiber, polyethylene, hollow polyester fiber, polypropylene (PP), jute fiber, rise husk, lignocelluloses, corn cob, hemp, flax, lignocelluloses produced from beech tree, pine, bamboo and banana fibers along with wool, and cotton and glass fibers were investigated as acoustic insulation materials [1–16]. Similarly, paraffine, eutectic organics, capric acid, expanded graphite, carbon fiber, polyethylene glycol, acrylic fiber, polyester fabrics, polyester-cotton fabrics, cotton fabrics, lyocell fabrics, poplar tree seed fiber, and bamboo fabrics were employed as thermal insulation materials [17–26].

Coating and laminating processes are often carried out in textile so as to provide textile materials with technical and functional properties. Furthermore, a variety of materials with different properties are combined through coating and laminating processes and their methods. The materials used and the coating resin determine the quality of fabrics produced. The fabrics coated and laminated have a variety of areas of use, ranging from agrotech, medtech, hometech, buildingtech to protective clothes [27].

In this study, production of multilayer surfaces providing acoustic and thermal insulation was investigated so as to provide insulation in buildings. After the optimum textile materials had been chosen aimed at acoustic and thermal insulation, surfaces were reinforced with pumice stone powder to develop the acoustic and thermal insulation properties of multilayer surfaces. Consequently, these surfaces were coated with an adhesive material in order to provide the wall with the property of multilayer surface adhesion. Consequently, porosity, air permeability, sound absorption coefficient, thermal conductivity coefficient, and adhesive properties of surfaces were investigated in accordance with the type of top layer of fabric, concentration, and particle size of pumice stone powder.

Experimental

Pumice stone

First, pumice stone was grinded by using a bead mill and pulverized pumice stone was sieved with pore sizes of 250 μm and 150 μm, respectively. Second, chemical

constituents and physical structure of this material was analyzed by using scanning electron microscope (SEM) and energy-dispersive X-ray spectroscopy (EDX) by using ZEISS/EVO 40 electron microscope. Furthermore, X-ray diffraction (XRD) spectra of pumice stone powder were recorded on Bruker D8 Advance X-ray diffractometer with Cu-Kα radiation at voltage of 40 kV and current of 30 mA. Figure 1 shows the chemical constituents of pumice stone.

Pumice stone consists of 54.29% oxygen, 26.50% calcium, 11.91% silisium, 4.79% carbon, 1.33% aluminum, and 1.27% iron. Figure 2 illustrates XRD spectra of pumice stone.

According to the XRD spectra results, the reflection peaks of pumice stone were $2\theta = \sim 26.68$ and $2\theta = \sim 5.20$. According to the XRD spectra results, the crystallinity index (Crl) of pumice stone was calculated in accordance with the Segnal empirical method by the following equation [28]

$$Crl(\ \%) = \frac{I_{002} - I_{am}}{I_{002} \times 100} \tag{1}$$

where I_{002} is the maximum intensity of the I_{002} of the pumice stone crystallographic form (I) at $2\theta = 26.68$, I_{am} is the intensity of diffraction of the amorphous material at $2\theta = \sim 5.20$. The crystallinity ratio of pumice stone was 80.50%.

Fabrics

The bottom layer of fabric was produced from four-slotted polyester (SPET) fiber as nonwoven fabric. Two different fabrics were used as the top layer of fabric, which were woven as plain weave from PP warp yarn and texture PP (TPP) weft yarn and were woven as plain weave from PP warp yarn and texture yarn produced from hollow TPP (HTPP) fiber. The properties of fabrics are given in Table 1.

Coating paste

In order to apply pumice stone powder to PP fabrics, polyurethane (PU)-based coating material was used as linking agent. Furthermore, in order to prepare coating paste, RUCO-COAT PU 1110 (Rudolf Duraner), RUCO-COAT FX 8011 (Rudolf Duraner), and RUCO-COAT TH 821 (Rudolf Duraner) were mixed. RUCO-COAT PU 1110 is water based and aliphatic polyether PU dispersion in anionic form. RUCO-COAT FX 8011 is blocked isocyanate cross-linking agent in anionic form. RUCO-COAT TH 821 is synthetic thickener, acrylate in anionic structure. The coating chemicals were purchased from Rudolf Duraner Incorporated Company, headquartered in Bursa, Turkey (hereinafter referred to as Rudolf Duraner Inc.). The chemical structure of PU is given in Figure 3.

PU dispersion and cross-linking agent were used in the ratio of 19:1. Then, pumice stone powder was added to paste prepared at the rate of 5%, 10%, and 15%, respectively, based on the weight of paste.

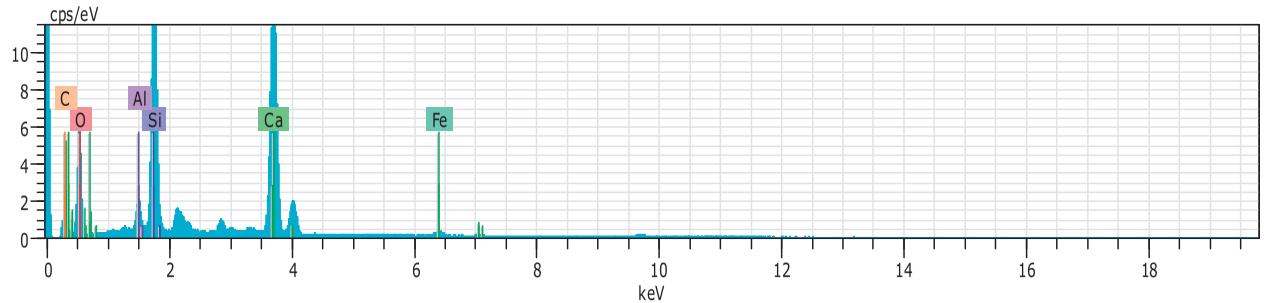

HV:20.0kV Puls th.:7.37kcps

El AN Series	unn. C [wt.%]	norm. C [wt.%]	Atom. C [at.%]	Error [%]
O 8 K-series	43.58	54.20	68.52	5.4
Ca 20 K-series	21.31	26.50	13.38	0.6
Si 14 K-series	9.58	11.91	8.58	0.4
C 6 K-series	3.85	4.79	8.07	0.7
Al 13 K-series	1.07	1.33	0.99	0.1
Fe 26 K-series	1.02	1.27	0.46	0.1
Total:	80.40	100.00	100.00	

Figure 1. Chemical constituents of pumice stone.

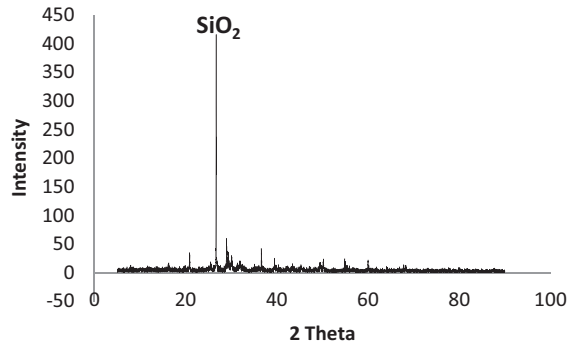

Figure 2. X-ray diffraction spectra of pumice stone.

Table 1. Properties of layers.

Sample code	Construction	Layer	Linear density weft (denier)	Linear density warp (denier)	Warp yarn density (threads/cm)	Weft yarn density (threads/cm)	Weight of fabrics (g/m^2)
SPET	Nonwoven	Bottom layer	–	–	–	–	496
TPP	Plain weave	Top layer	1100	2200	6	8	288
HTPP	Plain weave	Top layer	1100	2000	6	10	358

SPET: slotted polyester; HTPP: hollow texture polypropylene; TPP: texture polypropylene.

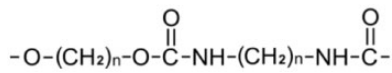

Figure 3. Chemical structure of polyurethane.

Gecko effect of coating paste

The adhesion characteristic of fabric was provided by using RUCO-COAT AC 2510 water based and polyacrylic ester dispersion in anionic–nonionic form purchased from Rudolf Duraner Inc. The chemical structure of polyacrylic ester is given in Figure 4.

Method

In this study, porosity, air permeability, sound absorption coefficient, thermal conductivity coefficient, and adhesive properties of surfaces consisting of two

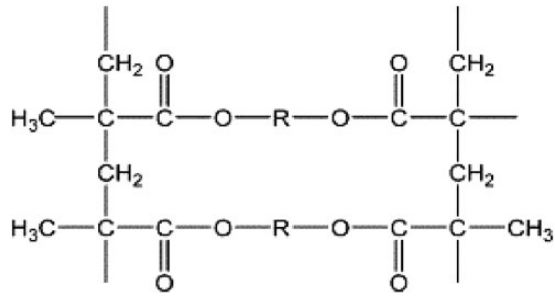

Figure 4. Chemical structure of polyacrylic ester [29].

fabrics, the mixture of PU/pumice stone powder, and polyacrylic ester-based material were investigated. First, water-repellent finishing process was applied to sublayers of fabrics produced from SPET fibers. Second, sublayers of fabrics were coated with the mixture of PU and pumice stone powder in order to promote insulation properties of fabrics. After surfaces had been combined with top layer of fabrics, the multilayer surfaces were coated with polyacrylic ester-based material to provide adhesion properties.

Water-repellent finishing process

Sublayer nonwoven fabrics were applied water-repellent finishing by using RUCO-DRY DFY fluorocarbon based and purchased from Rudolf Duraner Inc. in accordance with padding method so as to impede absorbing of sublayer of PU and polyacrylic coating materials. Afterwards, the fabrics were dried by using stenter drier (ATAC Lab. Machines GK40E) at 100°C for 5 min.

Coating

One side of sublayer of fabrics was coated with the mixture of the PU-based material and pumice stone powder by using laboratory coating machine (ATAC Lab. Machines RKL40). After the top layer of fabrics had been combined with the sublayer of fabrics, drying process was applied to multilayer surfaces by using stenter drier (ATAC Lab. Machines GK40E) at 110°C for 10 min. The part coated per square meter was approximately 275 g. After the combination of two surfaces, the other side of sublayer of fabrics was coated with polyacrylic ester-based material to promote adhesion characteristic by using laboratory type coating machine (ATAC Lab. Machines RKL40). The part coated with gecko per square meter was about 245 g. After coating, multilayer surfaces were cured by stenter drier (ATAC Lab. Machines GK40E) at 110°C for 7 min. The properties of the fabrics following coating processes are shown in Table 2.

Table 2. Properties of the fabrics following coating processes.

Sample code	Properties of surface
SPET+0%+TPP	Gecko coating + SPET + PU dispersion + TPP
SPET+0%+HTPP	Gecko coating + SPET + PU dispersion + HTPP
SPET+250 μm 5%+TPP	Gecko coating + SPET + PU dispersion + 250 μm 5% Pumice stone powder + TPP
SPET+250 μm 10 %+TPP	Gecko coating + SPET + PU dispersion + 250 μm 10% Pumice stone powder + TPP
SPET+250 μm 15%+TPP	Gecko coating + SPET + PU dispersion + 250 μm 15% Pumice stone powder + TPP
SPET+250 μm 5%+HTPP	Gecko coating + SPET + PU dispersion + 250 μm 5% Pumice stone powder + HTPP
SPET+250 μm 10%+HTPP	Gecko coating + SPET + PU dispersion + 250 μm 10% Pumice stone powder + HTPP
SPET+150 μm 5% + TPP	Gecko coating + SPET + PU dispersion + 150 μm 5% Pumice stone powder + TPP
SPET+150 μm 10%+TPP	Gecko coating + SPET + PU dispersion + 150 μm 10 % Pumice stone powder + TPP
SPET+150 μm 15%+TPP	Gecko coating + SPET + PU dispersion + 150 μm 15% Pumice stone powder + TPP
SPET+150 μm 5%+HTPP	Gecko coating + SPET + PU dispersion + 150 μm 5% Pumice stone powder + HTPP
SPET+150 μm 10%+HTPP	Gecko coating + SPET + PU dispersion + 150 μm 10% Pumice stone powder + HTPP
SPET+150 μm 15%+HTPP	Gecko coating + SPET + PU dispersion + 150 μm 15% Pumice stone powder + HTPP

SPET: slotted polyester; HTPP: hollow texture polypropylene; TPP: texture polypropylene; PU:polyurethane.

Calculation of porosity

The porosity of material was calculated using equation (2). The values of measurement of bulk density and density of sample skeletons were replaced in the following equation

$$h(\%) = \left(1 - \frac{\rho_m}{\rho_f}\right) \times 100 \tag{2}$$

where h represents porosity (%), ρ_m is the bulk density of sample (g/cm^3), and ρ_f is the density of sample skeletons (g/cm^3), respectively [30].

The measurement of air permeability

Measurements of air permeability were performed at the fabric surface of 20 cm^2 via determination of the amount of air for 1 s at 100 Pa pressure difference and the

results were stated in mm/s. The test was conducted in five different areas of multi-layer surfaces in accordance with TS 391 EN ISO 9237 standard [31] and the measuring instrument is shown in Figure 5. The measurements of air permeability were iterated 10 times.

Measurement of sound absorption coefficient

Sound absorption coefficient of materials was measured in accordance with ISO 10534-2 standard [32] by using a measuring instrument of Brüel & Kjaer Impedance Tube, which is based on two microphone transfer function method (Figure 6).

Figure 5. Testing instrument for air permeability.

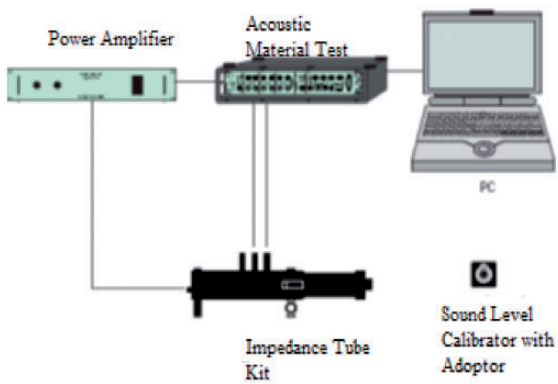

Figure 6. Impedance tube measuring instrument.

Brüel & Kjaer Impedance Tube consisted of two tubes whose diameters were 10 cm and 2.9 cm, respectively. The measurement of the material in the frequency range of 0–1600 Hz was conducted with the bigger tube, whereas the smaller tube was used for the measurement of the material in the frequency range of 600–6300 Hz. At one end of the tube, a loudspeaker was placed to function as a sound source. At the other end of the tube, the test material was situated so as to measure sound absorption properties. The measurements of sound absorption coefficient were iterated three times.

Measurement of thermal conductivity coefficient

Thermal conductivity coefficient of the samples was measured according to the TS 4512 Standard (TS 4512: Determination of Thermal Transmittance of Textiles, 1985) [33] by using P.A.HILTON LTD.H940 instrument shown in Figure 7. In order to measure thermal conductivity coefficient, samples with the diameter of 25 mm was primarily tested. Heat value (Q) in watt was noted from the digital screen of the instrument. The value of measurement of the thickness and the area of fabrics tested as well as heat difference were replaced in the following equation [34]

$$Q = -k.A.\frac{\mathrm{d}T}{\mathrm{d}x} \tag{3}$$

where Q represents heat flow (W), A is surface field (m^2), x is the thickness of sample (m), T is temperature difference (K), and k is thermal conductivity coefficient (W/m K). The measurements of thermal conductivity coefficient were iterated three times.

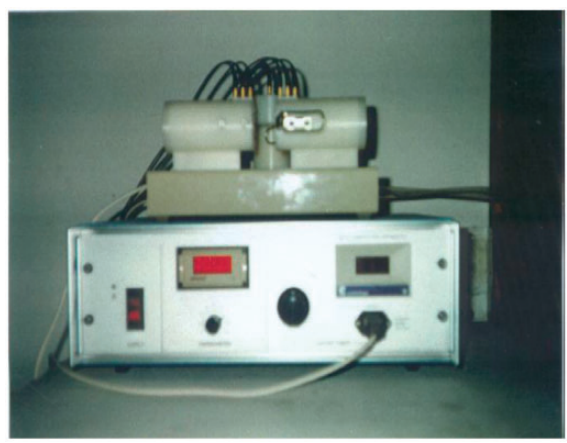

Figure 7. Testing instrument for heat transfer.

Results and discussion

Calculation of porosity

Multilayer surfaces contain PP, polyester, PU, polyacrylic ester, and pumice stone powder. Skeleton and bulk densities and porosity of multilayer surfaces are given in Table 3.

The results showed that porosity of multilayer surfaces increased with increasing concentration of pumice stone powder and with the decreasing particle size of pumice stone powder. The amount of pumice stone powder per meter square increased with the increasing concentration of pumice stone powder. Due to the microporous structure of pumice stone, the increase in the concentration of pumice stone caused the increase in microporosity of multilayer surfaces. In addition, the decrease in the particle size of pumice stone powder caused the increase in the sizes of air gaps among pumice stone particles. With regard to the results in terms of top layer of fabric, the porosity of multilayer surfaces including HTPP top layer of fabric was found to be higher than that of multilayer surfaces with TPP top layer of fabric. Moreover, the lumen layer in hollow PP fibers was considered to result in the increasing porosity of multilayer surface with HTPP top layer of fabric.

Table 3. Skeleton and bulk densities and porosity of multilayer surfaces.

Sample code	Skeleton density (g/cm^3)	Bulk density (g/cm^3)	Porosity (%)
SPET+0%+TPP	0.839	0.353	0.519
SPET+0%+HTPP	0.739	0.347	0.530
SPET+250 μm 5%+TPP	0.893	0.370	0.532
SPET+250 μm 10%+TPP	0.946	0.372	0.560
SPET+250 μm 15%+TPP	0.998	0.375	0.582
SPET+250 μm 5%+HTPP	0.794	0.373	0.559
SPET+250 μm 10%+HTPP	0.848	0.375	0.582
SPET+250 μm 15%+HTPP	0.899	0.378	0.602
SPET+150 μm 5%+TPP	0.904	0.350	0.534
SPET+150 μm 10%+TPP	0.968	0.354	0.567
SPET+150 μm 15%+TPP	1.031	0.357	0.594
SPET+150 μm 5%+HTPP	0.804	0.353	0.560
SPET+150 μm 10%+HTPP	0.869	0.356	0.590
SPET+150 μm 15%+HTPP	0.931	0.360	0.613

SPET: slotted polyester; HTPP: hollow texture polypropylene; TPP: texture polypropylene.

Measurement of air permeability of multilayer surfaces

In order to impede impairment of the wall onto which fabric was adhered due to airlessness, fabric produced was intended for enabling air permeability. Hence, air permeability of multilayer surfaces was analyzed and the results are given in Figures 8 to 12 pursuant to sublayer of fabrics, concentration, and particle size of pumice stone powder, respectively.

considering the results in terms of top layer of fabric demonstrates that air permeability of multilayer surface obtained from the top layer of fabric in which hollow PP fibers were used is higher than that of consisting of top layer of fabric

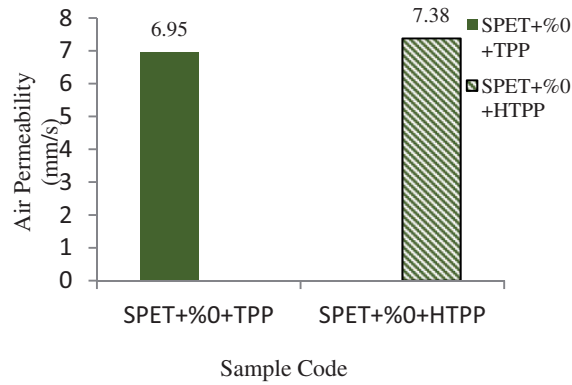

Figure 8. Air permeability of multilayer surfaces produced from different top layer of fabric.
SPET: slotted polyester; HTPP: hollow texture polypropylene; TPP: texture polypropylene.

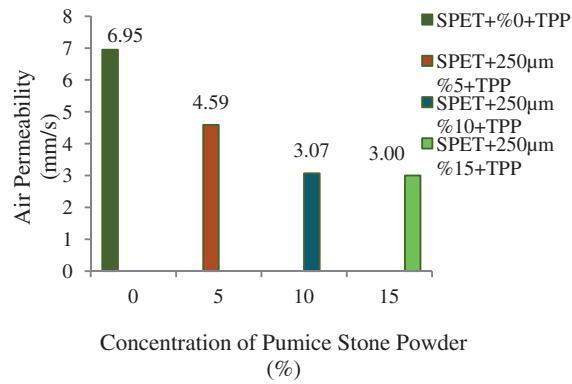

Figure 9. Air permeability of top layer of fabric woven from conventional PP fiber and 250 µm sized pumice stone powder.
SPET: slotted polyester; TPP: texture polypropylene.

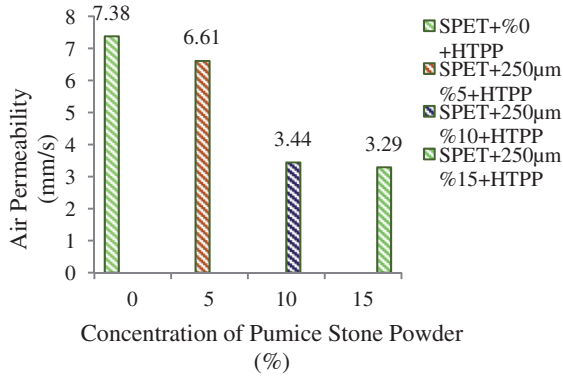

Figure 10. Air permeability of top layer of fabric woven from hollow PP fiber and 250 µm sized pumice stone powder.
SPET: slotted polyester; HTPP: hollow texture polypropylene.

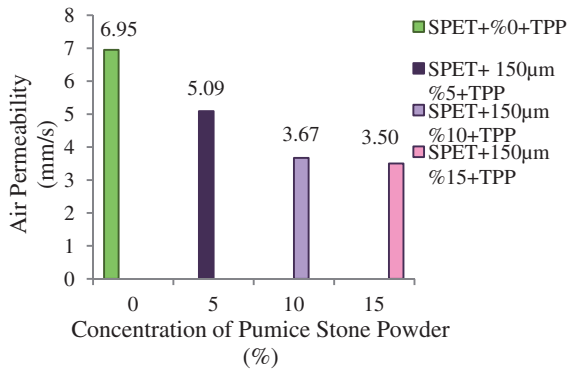

Figure 11. Air permeability of top layer of fabric woven from conventional PP fiber and 150 µm sized pumice stone powder.
SPET: slotted polyester; TPP: texture polypropylene.

obtained from conventional PP fiber was used. In particular, lumen layer in hollow PP fibers gave rise to the increase in air permeability of multilayer surfaces. The results of air permeability measurements show that air permeability of multilayer surfaces decreased with the increasing concentration of pumice stone powder, which, in turn, might result from filling the macro-sized pores in multilayer surfaces by the micrometer-sized pumice stone powder. Besides, the increase in the concentration of pumice stone powder was deemed to cause the increase in microporosity of multilayer surfaces. Also, air permeability of multilayer surfaces was increased with the decreasing particle size of pumice stone powder. In other words, as particle size of pumice stone decreases, so does the rate of closing macro-sized pores in pumice stone. In particular, micro-sized particles resulted in better air permeability

properties as opposed to macro-sized particles. Furthermore, porosity of samples increased with the decreasing sizes of pumice stone particles, which resulted from the increase in air permeability of multilayer surfaces.

Measurement of sound absorption coefficient of multilayer surfaces

Sound absorption coefficients of multilayer surfaces are given in Figures 13 to 17. Further, Figure 13 shows sound absorption coefficients of multilayer surfaces according to top layer of fabric.

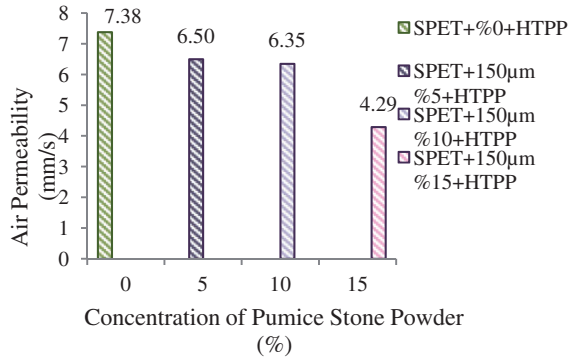

Figure 12. Air permeability of top layer of fabric woven from hollow PP fiber and 150 µm sized pumice stone powder.
SPET: slotted polyester; HTPP: hollow texture polypropylene.

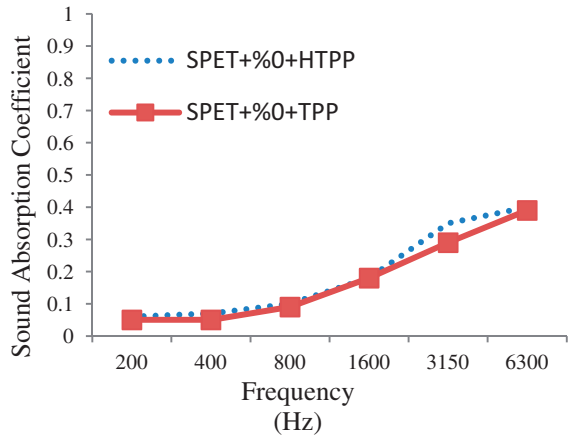

Figure 13. Sound absorption coefficients of multilayer surfaces produced from different top layers of fabric.
SPET: slotted polyester; HTPP: hollow texture polypropylene; TPP: texture polypropylene.

Upon consideration of the results in terms of top layer of fabric, sound absorption coefficients of multilayer surfaces consisting of the top layer of fabric in which hollow PP fibers had been used were noted to be higher than those of the multilayer surfaces in which the top layer of fabric obtained from conventional PP fiber had been used. Furthermore, porosity measurements showed that lumen layer in hollow PP fibers caused the increase in the amount of air within multilayer surfaces, whereas sound absorption coefficients of multilayer surfaces increased with the

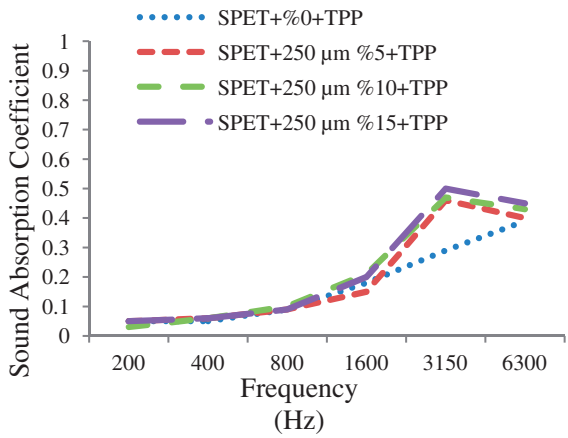

Figure 14. Sound absorption coefficients of top layer of fabric woven from conventional PP fiber and 250 µm sized pumice stone powder.
SPET: slotted polyester; TPP: texture polypropylene.

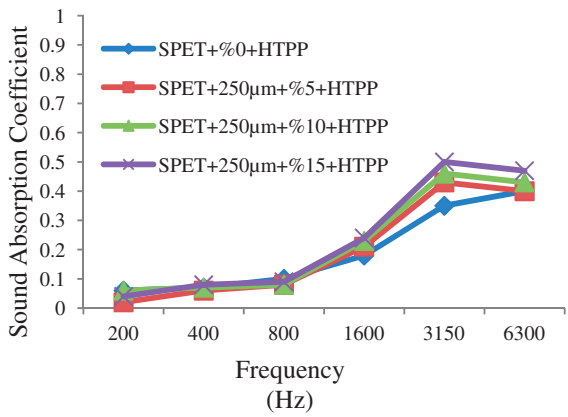

Figure 15. Sound absorption coefficients of top layer of fabric woven from hollow PP fiber and 250 µm sized pumice stone powder.
SPET: slotted polyester; HTPP: hollow texture polypropylene.

increasing porosity of surfaces. Besides, the thickness of multilayer surfaces consisting of the top layer of fabric in which hollow PP fibers (3.70 ± 0.05 mm) was negligibly higher than that of multilayer surfaces in which top layer of fabric obtained from conventional PP fiber (3.50 ± 0.05 mm) was used. Therefore, differences among the thicknesses of top layer of fabrics were deemed as not to influence sound absorption properties.

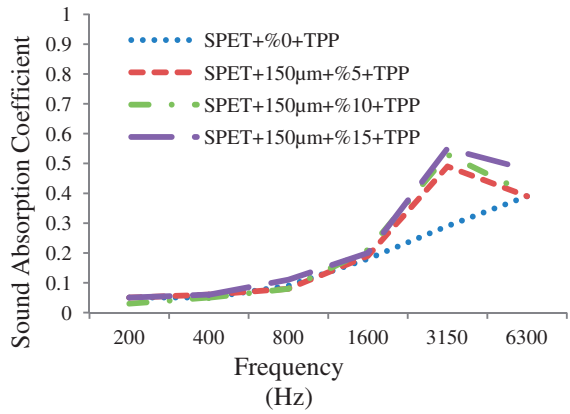

Figure 16. Sound absorption coefficients of top layer of fabric woven from conventional PP fiber and 150 μm sized pumice stone powder.
SPET: slotted polyester; TPP: texture polypropylene.

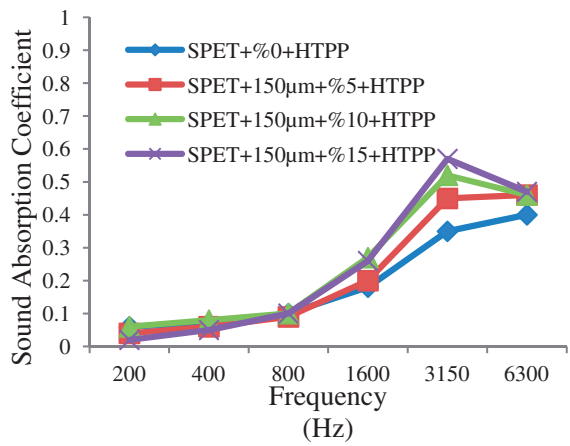

Figure 17. Sound absorption coefficients of top layer of fabric woven from hollow PP fiber and 150 μm sized pumice stone powder.
SPET: slotted polyester; HTPP: hollow texture polypropylene.

Figures 14 to 17 show sound absorption coefficients of multilayer surfaces in accordance with concentration and particle size of pumice stone powder.

The abovementioned values indicated considerable amount of differences between sound absorption coefficients of multilayer surfaces ranging from 100 to 1600 Hz frequency. The differences among sound absorption coefficients following 1600 Hz were investigated. Moreover, the results demonstrated that sound absorption coefficients of multilayer surfaces were lower at low frequencies, the reason of which was considered as the highness of the length of sound wave and lowness of the amplitude and, consequently, the ability to pass over the backside of the contacting surface of the sound was easy. Sound absorption coefficients of multilayer surfaces attained the maximum values at 3150–4000 Hz, the reason of which was deemed as the maximum sound absorption efficiency of multilayer surfaces, shortening the length of the sound waves, and increasing the amplitudes. Along with the increase in the amplitude, the increasing interactions between the sound waves and the absorbing surface were deemed to result in the increase in frictions and the amount of the sound energy which transformed into loss of heat energy. On the one hand, sample with the highest sound absorption coefficient in the frequency range of 1600–6300 Hz was the multilayer construction consisting of the top layer of fabric which was weaved from textured weft yarn, and which, in turn, was obtained from hollow PP fiber involving pumice stone powder in the concentration of 15% and in the particle size of 150 μm. On the other hand, sample weaved from textured PP weft yarn without including pumice stone powder had the lowest sound absorption coefficient in the abovementioned range. As a result of measurements of all the samples, one can conclude that sound absorption coefficient increased with the increasing concentration of pumice stone and the decreasing pumice stone particle size. Porosity of multilayer surfaces increased with the increasing concentration of pumice stone and the decreasing particle size of pumice stone. As the porosity of material increased, the capacity of sound absorption of material also increased. Furthermore, this increase resulted from the micropores, silicate, calcium oxide, iron oxide, and aluminum oxide within pumice stone. The microporous structure of pumice stone is shown in Figure 18.

Sound waves were transformed to loss of heat energy as a result of friction between sound waves and micro-sized air gaps. Furthermore, sound waves were absorbed by means of friction with the layer enclosing air gaps which was based silicate, calcium oxide, iron oxide, and aluminum oxide.

Moreover, sound absorption coefficients of multilayer surfaces were deemed to increase with the decreasing particle size of pumice stone because the roughness of surface increased. Consequently, frictions between sound and multilayer surfaces were considered to increase with the increasing surface roughness.

Measurement of thermal conductivity coefficients of multilayer surfaces

Thermal conductivity coefficients of multilayer surfaces were calculated according to the Fourier law. The area of samples was $4.91 \times 10^{-4} m^2$ and the thickness of the

multilayer construction in which textured PP weft yarn had been used as top layer of fabric was measured as 3.50 ± 0.05 mm, whereas the thickness of those in which textured yarn obtained from hollow PP fiber had been used as top layer of fabric was measured as 3.70 ± 0.05 mm by using James Heal Thickness Gauge measures. Figure 19 shows thermal conductivity coefficients of multilayer surfaces with respect to top layer of fabrics.

Upon consideration of the results in terms of top layer of fabrics, one can conclude that heat transfer coefficients of multilayer surfaces consisting of the top layer of fabric in which hollow PP fibers were used were higher than those

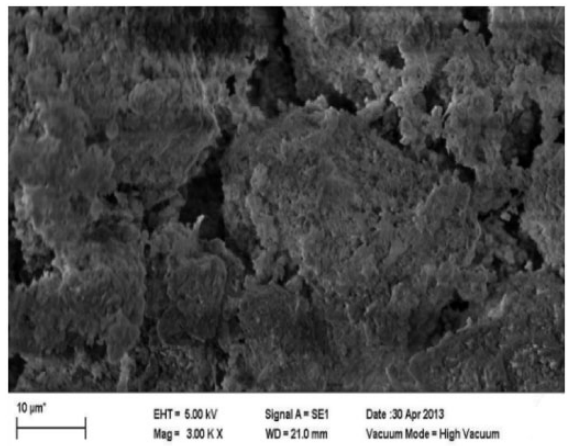

Figure 18. SEM image of pumice stone.

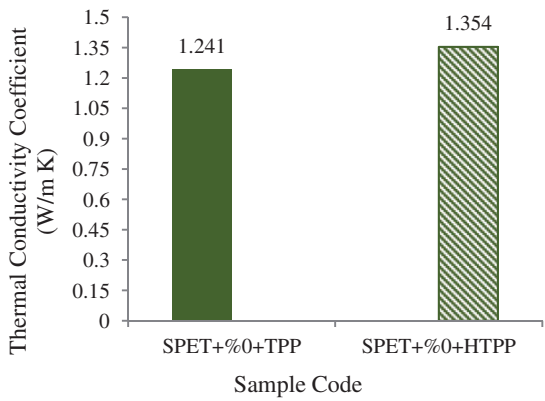

Figure 19. Thermal conductivity coefficients of multilayer surfaces produced from different top layer of fabrics.
SPET: slotted polyester; HTPP: hollow texture polypropylene; TPP: texture polypropylene.

of the multilayer surfaces in which the top layer of fabric obtained from conventional PP fiber was used. Another result was that thickness and density influenced thermal conductivity coefficients of samples. Furthermore, the results showed that the increase in density decreased thermal conductivity coefficient. The decrease in thickness gave rise to the increase in density. In more detail, the amount of fiber per square meter increased with the increasing density insomuch as the decrease in thickness in the same area. In other words, the increase in the amount of fiber could be deemed as the increase in density, which, in turn, was considered as the decrease in thermal conductivity coefficient. In general, thermal conductivity coefficient decreased with the increase in density of material [35].

Figures 20 to 23 show the thermal conductivity coefficients of multilayer surfaces with respect to concentration and particle size of pumice stone powder.

According to Figures 20 to 23, thermal conductivity coefficients of multilayer surfaces decreased with the increasing pumice stone powder. In particular, porosity, the amount of micropores, silicate, calcium oxide, iron oxide, and aluminum oxide increased with the increasing concentration of pumice stone powder per unit area. Silicate-based structure, composition, and the low thermal conductivity coefficient (0.080–0.12 W/m K) of pumice stone resulted in the decrease in thermal conductivity coefficients of multilayer surfaces. In addition, thermal conductivity coefficients of multilayer surfaces decreased with the decreasing particle sizes of pumice stone, resulting from the increase in porosity.

Table 4 illustrates thermal conductivity coefficients of the insulation materials in comparison with the samples with the lowest thermal conductivity coefficient at room temperature conducted in this study.

In this study, the comparison between samples with the optimum thermal conductivity and the former samples whose thermal conductivity coefficients were investigated indicated that samples with the optimum thermal conductivity

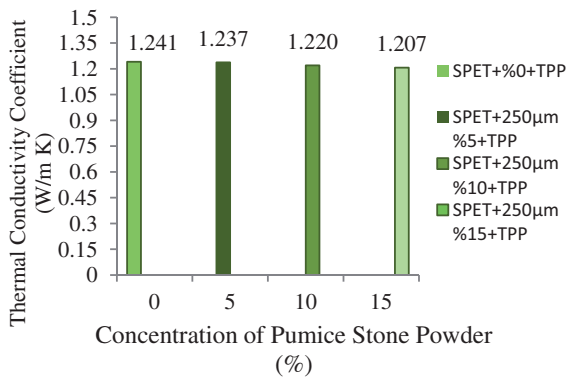

Figure 20. Thermal conductivity coefficients of top layer of fabrics woven from conventional PP fiber and 250 µm sized pumice stone powder.
SPET: slotted polyester; TPP: texture polypropylene.

coefficient were valued at high levels. More generally, thermal conductivity coefficient of materials does not only depend on density, temperature, and moisture of material but also depends on atomic, macromolecular, and chain structure as well as interaction with molecular chain or fiber [36].

Analysis of adhesion properties

In order to evaluate the adhesion behavior of technical fabrics produced, a testing apparatus was prepared. The samples were prepared in an area of 100 cm^2 so as to analyze the adhesion properties. Subsequently, these samples were adhered onto

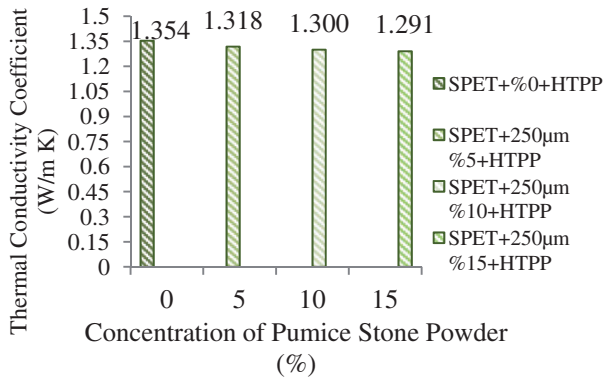

Figure 21. Thermal conductivity coefficients of top layer of fabrics woven from hollow PP fiber and 250 µm sized pumice stone powder.
SPET: slotted polyester; HTPP: hollow texture polypropylene.

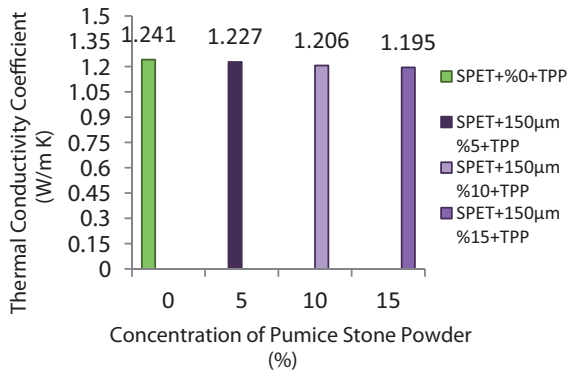

Figure 22. Thermal conductivity coefficients of top layer of fabrics woven from conventional PP fiber and 150 µm sized pumice stone powder.
SPET: slotted polyester; TPP: texture polypropylene.

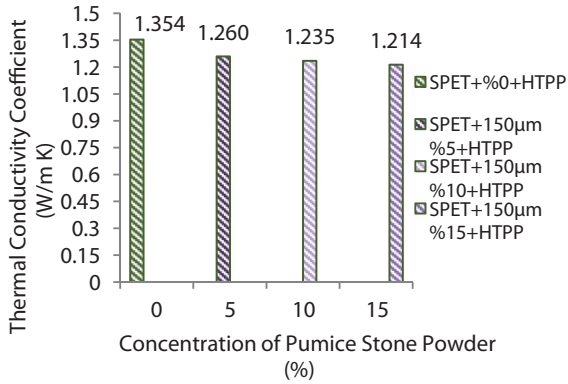

Figure 23. Thermal conductivity coefficients of top layer of fabrics woven from hollow PP fiber and 150 μm sized pumice stone powder.
SPET: slotted polyester; HTPP: hollow texture polypropylene.

Table 4. Thermal conductivity coefficients of the insulation materials in the former studies in comparison with those conducted in the latter studies.

Material	Density (kg/m^3)	Thermal conductivity coefficient (W/m K)
Molded polystyrene	19±1	0.034 [35]
Molded polystyrene	38±1	0.032 [35]
Fiberglass	27	0.0352 [36]
Fiberglass	47	0.0335 [36]
Rock wool	46	0.0397 [36]
Rock wool	120±1	0.037 [35]
SPET+150 μm %15+TPP	378±0.05	1.195

SPET: slotted polyester; TPP: texture polypropylene.

the wall and 2.5 kg mass was hanged for 60 min in the relative humidity of 65 ± 2% and at the temperature of 20 ± 2°C. Consequently, all the multilayer surfaces still maintained their adhesive position on the wall.

Conclusion

This study aimed the investigation of the effect of concentration and particle size of pumice stone and top layer of fabric type on porosity, air permeability, sound absorption, and thermal conductivity coefficient of multilayer surfaces. Upon research of the literature regarding the application of acoustic and thermal insulation, TPP yarn, SPET, and PP fiber were selected as the optimum raw materials.

The different surfaces produced from SPET and the TPP yarn, which was produced from conventional and hollow fiber were combined using PU-based material. On the other hand, pumice stone powder was used to promote acoustic and thermal insulation properties of multilayer surfaces. Furthermore, polyacrylic ester-based material was used to provide multilayer surfaces with the adhesion property. The use of wall fabric obtained from the abovementioned multilayer surfaces was intended. The measurements of air permeability of these surfaces point out to their porous structures. Moreover, porosity of multilayer surfaces decreases with the increasing concentration of pumice stone powder. In other words, porosity increases with the decreasing particle size of pumice stone powder. Consequently, air permeability, acoustic, and thermal insulation properties of multilayer surfaces were enhanced with the increase in concentration of pumice stone powder and the decrease in particle size of pumice stone. As a result, the increase of porousness at microdimensions, porosity, and the amount of composites within the structure of pumice stone per area of multilayer surfaces were concluded to enhance air permeability, acoustic, and thermal insulation of multilayer surfaces.

According to XRD analysis of pumice stone, one can conclude that the crystallinity index of pumice stone was high due to the lowness of the acoustic and thermal insulation capacity of multilayer surfaces. In addition, if pumice stone was more amorphous, the acoustic and thermal capacity of multilayer surfaces would be higher.

Consequently, these surfaces can be employed in buildings so as to provide acoustic and thermal insulation. Besides, these surfaces have adhesion to any surface as well as air permeability not to impair any surface arising out of airlessness.

Funding

This research received no specific grant from any funding agency in the public, commercial, or not-for-profit sectors.

References

[1] Sukontasukkul P. Use of crumb rubber to improve thermal and sound properties of precast concrete panel. *Construct Build Mater* 2009; 23: 1084–1092.
[2] Ersoy S and Küçük H. Investigation of industrial tea-leaf-fibre waste material for its sound absorption properties. *Appl Acoust* 2009; 70: 215–220.
[3] Jiang S, Xu Y, Zhang H, et al. Seven-hole hollow polyester fibers as reinforcement in sound absorption chlorinated polyethylene composites. *Appl Acoust* 2012; 73: 243–247.
[4] Yang TL, Chiang DM and Chen R. Development of a novel porous laminated composite material for high sound absorption. *Text Res J* 2001; 7: 675–698.
[5] Fatima S and Mohanty AR. Acoustical and fire-retardant properties of jute composite materials. *Appl Acoust* 2011; 72: 108–114.
[6] Yang HS, Kim DJ and Kim HJ. Rice straw–wood particle composite for sound absorbing wooden construction materials. *Bioresource Technol* 2003; 86: 117–121.
[7] Zhou J, Zheng L and Lu H. An environment-friendly thermal insulation material from cotton stalk fibers. *Energy Build* 2010; 47: 1070–1074.

[8] Huda S and Yang Y. A novel approach of manufacturing light-weight composites with polypropylene web and mechanically split cornhusk. *Ind Crops Prod* 2009; 30: 17–23.
[9] Markiewicz E, Paukszta D and Borysiak S. Acoustic and dielectric properties of polypropylene-lignocellulosic materials composites. *Polypropylene InTech* 2012; 193–217.
[10] Huda S and Yang Y. Composites from ground chicken quill and polypropylene. *Compos Sci Technol* 2008; 68: 790–798.
[11] Seddeq HS, Aly NM, Marwa A, et al. Investigation on sound absorption properties for recycled fibrous materials. *J Ind Text*. Epub ahead of print 7 May 2012. DOI: 10.1177/1528083712446956.
[12] Zou Y, Huda S and Yang Y. Lightweight composites from long wheat straw and polypropylene web. *Bioresource Technol* 2010; 101: 2026–2033.
[13] Reddy N and Yang Y. Light-weight polypropylene composites reinforced with whole chicken feathers. *J Appl Polym Sci* 2010; 116: 3668–3675.
[14] Lou CW, Lın JH and Su KH. Recycling polyester and polypropylene nonwoven selvages to produce functional sound absorption composites. *Text Res J* 2005; 75: 390–394.
[15] Liang JZ and Jiang XH. Soundproofing effect of polypropylene/inorganic particle composites. *Composites: Part B* 2012; 43: 1995–1998.
[16] Parıkh DV, Calamarı TA, Sawhney APS, et al. Thermoformable automotive composites containing kenaf and other cellulosic fibers. *Text Res J* 2002; 72: 668–672.
[17] Wang FZ, Wanga B, Ding XM, et al. Effect of temperature and structure on the free volume and water vapor permeability in hydrophilic polyurethanes. *J Membr Sci* 2002; 241: 355–363.
[18] Chen Y, Wang R, Zhou J, et al. Membrane formation temperature-dependent gas transport through thermosensitive polyurethane containing in situ-generated TiO_2 nanoparticles. *Polymer* 2011; 52: 1856–1865.
[19] Aydın AA and Okutan H. High-chain fatty acid esters of myristyl alcohol with odd carbon number: Novel organic phase change materials for thermal energy storage. *Solar Energy Mater Solar Cells* 2011; 95: 2417–2423.
[20] Sarı A and Karaipekli A. Preparation, thermal properties and thermal reliability of capric acid/expanded perlite composite for thermal energy storage. *Mater Chem Phys* 2007; 109: 459–464.
[21] Karaipekli A, Sarı A and Kaygusuz K. Thermal conductivity improvement of stearic acid using expanded graphite and carbon fiber for energy storage applications. *Renew Energy* 2007; 32: 2201–2210.
[22] Brigasa A, Nascimento D, Teixeira N, et al. Textile waste as an alternative thermal insulation building material solution. *Construct Build Mater* 2013; 38: 155–160.
[23] Saleh SS. Performance of needle-punching lining nonwoven fabrics and their thermal insulation properties. *J Basic Appl Sci Res* 2011; 1: 3513–3524.
[24] Matusiak M and Sikorski K. Influence of the structure of woven fabrics on their thermal insulation properties. *Fibres Text Eastern Eur* 2011; 19: 46–53.
[25] Frydrych I, Dziworska G and Bilska J. Comparative analysis of the thermal insulation properties of fabrics made of natural and man-made cellulose fibres. *Fibers Text East Eur* 2002; 10: 40–44.
[26] Chen HL and Cluver B. Assessment of poplar seed hair fibers as a potential bulk textile thermal insulation material. *Cloth Text Res J* 2010; 28: 255–262.
[27] Bulut Y and Sular V. General properties and performance tests of fabrics produced by coating and lamination techniques. *J Text Eng* 2010; 70–71: 5–16.

[28] Kocak D. The study of the effects of different chemical compounds applied on luffa cylindrical fibers with the help of ultrasonic energy. *J Polym Eng* 2008; 28: 501–515 [Reviewer III].
[29] Pan B, Pan B, Zhang W, et al. Development of polymeric and polymer-based hybrid adsorbents for pollutants removal from waters. *Chem Eng J* 2009; 151: 19–29.
[30] Voronina N. Acoustic properties of fibrous material. *Appl Acoust* 1994; 42: 165–174.
[31] TS 391 EN ISO 9237 Standard. *Determination of air permeability of fabric*, 1995.
[32] ISO 10534-2 Standard. *Acoustics – determination of sound absorption coefficient and impedance in impedance tubes – Part 2: Transfer-function method*, 1998.
[33] TS 4512 Standard. *Determination of heat transfer coefficient of textile materials*, 1985.
[34] Kılıç M and Yigit A. *Isı transferi*. Bursa: Alfa Aktuel, 2008.
[35] Al-Ajlan SA. Measurement of thermal properties of insulation materials by using transient plane source technique. *Appl Therm Eng* 2006; 26: 2184–2191.
[36] Abdou A and Budaiwi I. The variation of thermal conductivity of fibrous insulation materials under different level of moisture content. *Construct Build Mater* 2013; 43: 533–544.